JCTC Journal of Chemical Theory and Computation

pubs.acs.org/JCTC Article

# A Python Algorithm to Analyze Inelastic Neutron Scattering Spectra Based on the *y*-Scale Formalism

Claudia Scatigno, Giovanni Romanelli,* Enrico Preziosi, Matteo Zanetti, Stewart F. Parker, Svemir Rudić, Carla Andreani, and Roberto Senesi

Cite This: https://dx.doi.org/10.1021/acs.jctc.0c00790 Read Online

ACCESS | Metrics & More | Article Recommendations

**ABSTRACT:** This paper presents a Python-based algorithm, named INSCorNorm, to correct the inelastic neutron scattering (INS) spectra for both sample and container self-shielding and to normalize the experimental spectral intensity to an absolute physical scale (barn/energy unit) facilitating the comparison with computer simulations and interpretation. The algorithm is benchmarked against INS measurements of $ZrH_2$ performed on the TOSCA spectrometer at the ISIS Facility. We also apply the algorithm to the INS spectra from L-lysine, a system of broad interest in biology and medicine, and we discuss how corrected INS data provide an experimental benchmark for theoretical calculations of nuclear anisotropic displacement parameters in molecular systems. The total neutron sample cross section to use for the self-shielding corrections is discussed, as well as the best approach to derive experimentally the cross section at the VESUVIO spectrometer, together with the experimental value of the hydrogen nuclear mean kinetic energy, $\langle E_k \rangle$. The algorithm is made available to the neutron user community within the MANTID software.

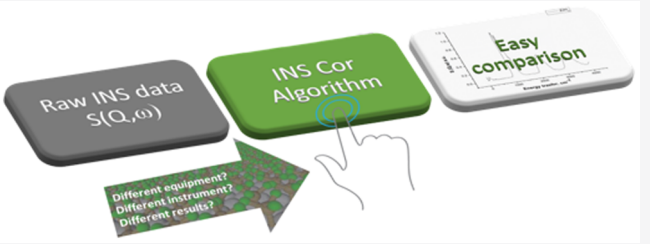


## 1. INTRODUCTION

Neutron vibrational spectroscopy (inelastic neutron scattering, INS) is a well-established experimental technique that probes the atomic-scale dynamics of condensed matter systems.[1,2] All vibrational modes are allowed, and their spectral intensity depends on the total scattering cross section and the amplitude of motion of the atoms involved in the mode. The INS physical process consists of an exchange of energy between neutrons and nuclei resulting in the excitation of a phonon or a lattice or molecular vibration in the sample under investigation. Neutrons impinging on the system can lose a fixed amount of energy in such a process, equal to the excitation energy of the vibration, and the spectra resulting from an INS experiment are representative of the vibrational density of states of the system.

INS spectrometers at spallation neutron sources, such as the ISIS Pulsed Neutron and Muon Source (Didcot, UK), use time-of-flight (TOF) methods for energy analysis. This requires that either the energy of the incident or the scattered neutron is known. These are known as direct and indirect geometry spectrometers, respectively. Indirect geometry spectrometers exploiting INS are generally used to observe the low-energy transfer range, *i.e.*, spectral features below 200 meV (1 meV $\simeq$ 8.065 $cm^{-1}$), where lattice and low-energy vibrational modes manifest themselves. The TOSCA beamline at ISIS has been a gold standard for INS for the last two decades, as demonstrated by the TOSCA INS database[3] and the recent International Review.[4] Moreover, the instrument capabilities have been significantly enhanced following the installation of a neutron guide,[5,6] the upgrade of the beryllium filters,[7] and the ability to exploit the empty pulse resulting from ISIS TS2 operation, giving access to the elastic line and extending the energy transfer range to as low as −3 meV (*i.e.*, the "anti-Stokes" side of the elastic line).[7] Given the large cross section of hydrogen (82.03 barn), the INS technique is particularly suitable to study hydrogenous compounds where the scattering of neutrons is dominated by hydrogen. $ZrH_2$ is often used as a reference material owing to its simple, reproducible, and well-known behavior: it allows a full assignment in terms of fundamental, overtone,[8] and combination modes.[9]

INS experimental results can be readily compared with the INS spectra generated from single-molecule or periodic DFT calculations. However, it is rare to express the experimental data on an absolute intensity scale. The current practice is to scale the calculated spectrum to match the experimental one. If the experimental data were on an absolute scale, this would remove an arbitrary procedure. The use of an absolute scale

Received: July 29, 2020

would also facilitate data curation: instruments usually evolve over the course of a typical 20 year lifespan and the comparison of the spectra from different versions of the same instrument is not necessarily straightforward. The comparison of the spectra from nominally similar instruments at different institutions is even more problematic. Recently, a novel normalization procedure for INS data has been suggested,[10] which is based on the $y$-scaling[11,12] formalism within the framework of the impulse approximation (IA).[13,14] The latter is valid at high values of energy transfer, $E_T$, and wave vector, $Q$,.[12,14] This is the deep inelastic neutron scattering (DINS) regime,[15,16] where the VESUVIO instrument[17−22] at ISIS operates to measure nuclear mean kinetic energies, $\langle E_k \rangle$, and momentum distributions, $n(p)$, of light[14] and heavy nuclei.[15] This novel procedure requires knowledge of the energy-dependent total neutron cross section of the sample under investigation and the value of $\langle E_k \rangle$.

The energy-dependent total neutron cross sections, $\sigma(E)$, is a physical quantity[23−26] related to the structure and dynamics of a sample at the microscopic scale. Measurements of $\sigma(E)$ can be performed using broad-band neutron transmission at the VESUVIO spectrometer[27−29] in the energy range meV−keV, concurrently with the DINS experiment.

In this paper, we present the algorithm INSCorNorm that allows container and self-shielding corrections of INS data collected at the TOSCA spectrometer. It provides a physical and intrinsic normalization of the data based on the discussion in ref 10. The latter introduces the use of an approximated model for $\sigma(E)$, namely, the free hydrogen gas (FHG), and an approximate estimate for the hydrogen $\langle E_k \rangle$ for the normalization. Here, we go beyond these approximations by proposing the use of both the experimental quantities, $\sigma(E)$ and $\langle E_k \rangle$, measured on the VESUVIO spectrometer. An additional model for $\sigma(E)$ for hydrogen in organic molecules[25] is also implemented within the algorithm, to be employed for similar samples in cases where the experimental cross section is not available. We benchmark the new algorithm to the case of $ZrH_2$, a suitable analyte wherein the hydrogen dynamics can be approximated using an isotropic and harmonic potential with a fundamental transition energy of ca. 140 meV.[30,31] Moreover, we apply the algorithm to the case of the essential amino acid L-lysine,[32] a compound of interest in both biology[33] and soft matter.[34]

## 2. MATERIALS AND METHODS

Experiments were performed on commercially available powder samples of $ZrH_2$. Two samples with different amounts and thicknesses were used, as shown in Table 1. Additional measurements on L-lysine, discussed in Section 4.1, shared the same experimental details presented below.

**Table 1. Experimental Details for the $ZrH_2$ and L-Lysine Samples: Thickness of the Sample, Mass of the Samples, and Integrated Proton Charge, IPC ($\mu$Ah), Related to the TOSCA and VESUVIO Measurements**

| parameter | sample 1 | sample 2 | L-lysine |
|---|---|---|---|
| thickness (cm) | 0.100 | 0.244 | 0.100 |
| mass (g) | 5.357 | 9.434 | 2.698 |
| $IPC_{TOSCA}$ ($\mu$Ah) | 169 | 600 | 200 |
| $IPC_{VESUVIO}$ ($\mu$Ah) | 3600 | 3600 | 3060 |

The measurements were carried out using TOSCA for INS[31] (Figure 1) and VESUVIO[35] for neutron transmission and DINS. Standard flat Al cells, 4.0 × 4.8 $cm^2$ in size, were used for both experiments. Taking into account the TOSCA beam size,[5] the amounts of sample in the beam were 98 and 78% for sample 2 and sample 1, respectively, as determined by neutron radiography.

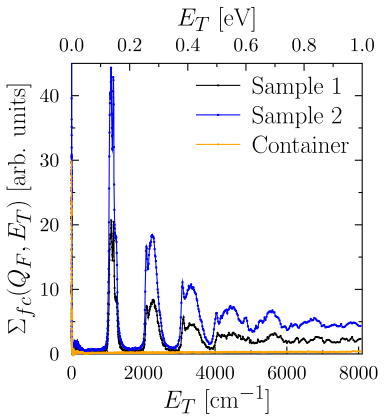


**Figure 1.** Experimental filled-container INS spectra, $\Sigma_{fc}(Q_F, E_T)$ of both $ZrH_2$ samples (sample 1, black line, sample 2, blue line). The spectrum from the empty container, $\Sigma_{ec}(Q_F, E_T)$, is also shown (orange line).

The TOSCA instrument is an inverted-geometry TOF spectrometer with a wide range of energy transfer ($E_T$), between −3 and 1000 meV, and angular coverage over two fixed dynamic trajectories (*i.e.*, back scattering and forward scattering). Neutrons scattered from the sample are Bragg-reflected from a pyrolytic graphite analyser (HOPG) toward the detectors, with a final average neutron energy of $E_f \simeq 4$ meV. Experiments on TOSCA are routinely performed by placing the sample into a top-loading closed-cycle refrigerator (CCR) kept at a base temperature of about 10 K and in the environment of 10 mbar of helium gas used to facilitate the sample cooling via heat exchange with the CCR walls. The INS detector banks have five analyser modules in back-scattering direction ($\theta_B \simeq 135°$) and five in the forward-scattering ($\theta_F \simeq 45°$) direction. The instrument is characterized by its 17 m primary flight path and approximately 4 × 4 $cm^2$[36] beam size at the sample position,[7] taken as the full width at half-maximum of the beam profile.

The VESUVIO spectrometer is a TOF instrument that records neutrons scattered between 30 and 70° in forward scattering and between 130 and 170° in back scattering.[27,37−39] Neutrons scattered along the hydrogen recoil line cover the $Q$ range 30−200 $Å^{-1}$. DINS experiments on VESUVIO allow the measurement of atomic momentum distributions and nuclear mean kinetic energies in condensed matter systems[15,16] (see Section 3.2). For concurrent neutron transmission measurements,[28] the monitors, Li-doped glass scintillators, are located at 13.43 m (after the sample) and 8.60 m (before the sample) from the moderator, along the beam direction. The sample is placed in a CCR at 11 m from the moderator. Transmission and DINS experiments on VESUVIO were performed using the same samples (and containers) following the measurements on TOSCA, and the transmission spectra were analyzed in the same range of incident energies as for the INS spectra.


https://dx.doi.org/10.1021/acs.jctc.0c00790
J. Chem. Theory Comput. XXXX, XXX, XXX−XXX

## 3. CORRECTION AND NORMALIZATION ALGORITHM

The INSCorNorm algorithm corrects the INS spectra for empty container and sample self-shielding and finally normalizes the spectra to a physical scale of barn/energy unit. The latter quantity corresponds to the double differential scattering cross section averaged over the angular solid angle related to the position of the detectors. In the case of TOSCA-type instruments, this corresponds, in practice, to two narrow scattering angles, one for the forward and one for the backward detector banks. However, the algorithm can be easily generalized so as to normalize each detector separately, thus providing a punctual angular information for instruments with different detector geometries.

In this section, a detailed description of the corrections is provided, then the normalization procedure is discussed, and finally an explanation on how the theory is translated into the proposed algorithm is given. The procedure was suggested in ref 10 from where we adopt a simplified notation. The signal from the sample within the container can be expressed as

$$\Sigma_{fc}(E_T) = T_c(0)S(\theta_{F,B}, E_i, E_f)T_c(\theta_{F,B})\Sigma_s(Q_{F,B}, E_T) + (T_s(0, E_i)T_c(0) + T_s(\theta_{F,B}, E_f)T_c(\theta_{F,B}))W(Q_{F,B}, E_T) \quad (1)$$

while, for the empty container, the experimental signal can be expressed as

$$\Sigma_{ec}(E_T) = (T_c(0) + T_c(\theta_{F,B}))W(Q_{F,B}, E_T) \quad (2)$$

Here, $\Sigma_s(Q_{F,B}, E_T)$ is the macroscopic self-scattering law for the sample, including the convolution with instrumental resolution, $S(Q_{F,B}, E_T)$ is the sample self-shielding function, while $T_s(\theta, E)$ and $T_c(\theta)$ are the sample and container attenuation functions, respectively. Finally, $W(Q_{F,B}, E_T)$ is the signal coming from one container wall (not corrected for its own self-shielding). In this procedure, the sample transmission is taken as a function of the neutron energy, either before or after the scattering event, while the transmission of the empty container is taken as a constant function of the neutron energy. One should notice that, for the majority of neutron experiments, the container is manufactured either with Al or with other low-scattering materials, and its attenuation for eV neutrons is of the order of few percent. For cold and thermal neutrons, the features in the attenuation function are primarily driven by Bragg edges that are considered negligible for such thin containers. Finally, differing from ref 10, any multiple scattering contributions at this stage have been neglected. Figure 1 shows the experimental signals for the two $ZrH_2$ samples in the container, $\Sigma_{fc}$, and for the empty container, $\Sigma_{ec}$.

### 3.1. Corrections for Attenuation and Self-Shielding.

The energy-dependent attenuation of neutrons through the sample is a function of the energy-dependent cross section and of the sample geometry. It can be obtained in neutron transmission measurements interpreted via the Beer−Lambert law, whereby the transmission spectrum as a function of the incident neutron energy, $T(E)$, is related to $\sigma(E)$ as

$$T(E) = \exp(-n_H\sigma(E)) \quad (3)$$

with the areal density of hydrogen atoms ($n_H$) defined from the mass of sample inserted in the container ($m$), the container surface ($A$), the molar mass of the same formula unit to which the cross section refers to ($M$), and the number of hydrogen atoms per formula unit ($N_H$),

$$n_H = \frac{N_H m}{MA\mu} \quad (4)$$

If $m$ is expressed in g, $A$ in $cm^2$, and $M$ in amu, one can use $\mu = 1.66054$ to obtain $n_H$ in $barn^{-1}$. Figure 2 shows the

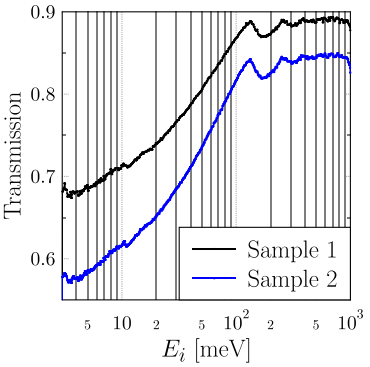


**Figure 2.** Experimental neutron transmission of $ZrH_2$ as a function of the incident neutron energy, as measured on the VESUVIO spectrometer: sample 1 (black line) and sample 2 (blue line).

experimental neutron transmission from the two samples of $ZrH_2$, as measured on VESUVIO. By comparison with the INS spectra shown in Figure 1, one can appreciate how the features in $T(E)$, thus in $\sigma(E)$, are closely related to the probability to excite a vibration in the INS spectra. The low-energy region is dominated by the incoherent elastic scattering from hydrogen; the following features at ca. 140, 280 meV, etc., correspond, within the framework of the multiphonon expansion of the dynamic structure factor, to the 1-phonon and 2-phonons terms, respectively.

Qualitative inspection of Figure 2 delivers two clear messages. First, the transmission function, thus the sample attenuation, is sample-dependent: the position and intensity of the features in the total scattering cross section are strictly related to the vibrations taking place at the microscopic level. These are especially noticeable for hydrogenous samples. Second, by comparing the spectral intensity for the two samples with the value of $ZrH_2$ cross section available in the literature, one can notice how the Beer−Lambert law only applies if the bulk density of the samples, 5.6 g/mL, is replaced with a preparation-dependent powder density. As a consequence, in order to perform as accurate corrections as possible of the INS data, an experimental determination of the transmission is needed.

One can also notice that eqs 1 and 2 require the determination of both the transmission of the sample for incident neutrons impinging on the sample at $\theta = 0$ and for scattered neutrons at a generic angle $\theta$. While the neutron transmission measurement allows the direct determination of $T(0, E) \equiv T(E)$, one can obtain $T(\theta, E)$ assuming that the values of density and cross section remain the same for scattered neutrons, yet the thickness of the neutron path in the sample increased. Therefore, the following relation is used in the algorithm:

$$T(\theta, E) = \exp\left(\frac{\ln T(0, E)}{\cos\theta}\right) \quad (5)$$


https://dx.doi.org/10.1021/acs.jctc.0c00790
J. Chem. Theory Comput. XXXX, XXX, XXX−XXX

Considering that in many cases it is not possible to determine the experimental cross section or, more importantly, the experimental transmission of the sample in the INS experiment, three options are available:

- experimental transmission data obtained concurrently with the INS measurement, over the same INS energy range, or on broad band spectrometers like VESUVIO. This is the best choice when available for it takes into account the real neutronic response and density of the sample;
- the averaged organic molecular systems cross section by Capelli and Romanelli.[25] This is an experimentally determined total cross section for hydrogen, averaged over a series of organic systems. In this case, the hydrogen dynamics, thus the cross section, is dominated by the molecular internal modes based on OH, CH, and NH bonds;
- the FHG model, as suggested in ref 10. This approach is representative of an ideal case whereby hydrogen atoms are not interacting, and their dynamics is solely driven by temperature-defined translational modes. This is an approximate model for the total neutron cross section, which can be expressed in a simple analytical form, yet suffering from nonphysical divergence of the cross section for vanishing incident energy. By defining an effective temperature of the FHG, $T^*$, *e.g.*, proportional to the nuclear mean kinetic energy, one can approximately take into account the hydrogen dynamics: for example, the effective temperatures of liquid water at room temperature and ice at 269 K are approximately 1130 and 1207 K, respectively,[40,41] and this value will change depending on confinement and other thermodynamic variables.[42−44] The FHG cross section can be expressed as

$$\sigma_{\mathrm{FHG}}(E) = \frac{\sigma_b}{4\epsilon}\left[\left(\epsilon + \frac{1}{2\epsilon}\right) erf(\epsilon) + \frac{\exp(-\epsilon^2)}{\sqrt{\pi}}\right] \quad (6)$$

where $\epsilon = E/k_B T^*$ and $k_B$ is Boltzmann's constant. The limitations of this model will be discussed later.

One should notice that approximated values of $\langle E_k \rangle$ and $T^*$ can be obtained self-consistently from a simulated vibrational density of states, $g(E_T)$ as[10,14,15]

$$\frac{3}{2}k_B T^* = \langle E_k \rangle = \frac{1}{4}\int E_T g(E_T) \coth\left(\frac{E_T}{2k_B T}\right) \quad (7)$$

As far as the self-shielding correction is concerned, the following analytical approximation for a flat-geometry sample[45] have been used, respectively, for forward scattering (transmission geometry):

$$S(\theta_F, E_i, E_f) = \frac{T(0, E_i) - T(\theta_F, E_f)}{\log(T(0, E_i)) - \log(T(\theta_F), E_f)} \quad (8)$$

and back scattering (reflection geometry):

$$S(\theta_B, E_i, E_f) = \frac{T(0, E_i)T(\theta_B, E_f) - 1}{\log(T(0, E_i)) + \log(T(\theta_B), E_f)} \quad (9)$$

If the transmission function is obtained from a model cross section, one needs to provide an estimate of the areal density. If the experimental value of the transmission function is available, the areal density is included in the transmission data. While the previous formalism holds in the case of flat-geometry containers, generally used on indirect-geometry INS spectrometers, the MANTID environment includes other Monte-Carlo-based algorithms to evaluate the self-attenuation correction for other sample geometries that can be used within INSCorNorm if necessary.

**3.2. Normalization of the Spectra.** The normalization procedure follows and expands on what was introduced in ref 10. It assumes the validity of both the multiphonon expansion[46] for thermal neutrons and the IA for epithermal neutrons, in the range of energy transfer 600 meV−1 eV.

Within the IA,[11,15] the nucleus is considered a non-interacting particle recoiling freely after a scattering event. The energy transfer, $E_T$, is therefore centered around the recoil energy, $E_R$, inversely proportional to the nuclear mass, $M$, and proportional to the square of the wave vector, $Q$

$$E_T = \frac{\hbar^2 Q^2}{2M} + \frac{\hbar \vec{Q}\cdot\vec{p}}{2M} = E_R + \frac{\hbar^2 Q}{M} y \quad (10)$$

where $\vec{p}$ is the momentum of the nucleus before the scattering event, and $y = \vec{p}\cdot\hat{Q}/\hbar$ is its projection along the direction of the momentum transfer. Before the scattering event, the dynamics of the nucleus depends on the molecular or crystalline vibrational modes, with a mean kinetic energy $\langle E_k \rangle = 3\hbar^2\sigma_p^2/2M$, with $\sigma_p$ being the standard deviation of the nuclear momentum distribution $\sigma_p^2 = \langle y^2 \rangle$. The nuclear momentum distribution can be accessed in a DINS experiment via the neutron Compton profile (NCP),[14,15] and for a system described by a harmonic and isotropic potential, it can be written as

$$S_{\mathrm{IA}}(Q, E_T) = \frac{M}{\hbar^2 Q} J(y) = \frac{M}{\hbar^2 Q} \frac{\exp\left(-\frac{y^2}{2\sigma_p^2}\right)}{\sqrt{2\pi\sigma_p^2}} \quad (11)$$

By replacing $y = \frac{M}{\hbar Q}(E_T - E_R)$, one gets the familiar expression of the dynamic structure factor for a gas of free nuclei

$$S_{\mathrm{IA}}(Q, E_T) = \frac{\exp\left(-\frac{3(E_T - E_R)^2}{8\langle E_k \rangle E_R}\right)}{\sqrt{8\pi E_R \langle E_k \rangle/3}} = \frac{\exp\left(-\frac{(E_T - E_R)^2}{2E_R\hbar\omega_0}\right)}{\sqrt{2\pi E_R \hbar\omega_0}} \quad (12)$$

where the last equality only holds for a single harmonic oscillator of frequency $\omega_0$, *i.e.*, for a harmonic and isotropic potential. This is a satisfactory approximation for $ZrH_2$, where $\hbar\omega_0 \simeq 140$ meV.

The connection between the IA and the multiphonon expansion was already discussed by Watson[47] for a similar system with only one phonon frequency, with the result

$$S_{\mathrm{MP}}(Q, E_T) = e^{-E_R/\hbar\omega_0} \sum_n \frac{1}{n!}\left(\frac{E_R}{\hbar\omega_0}\right)^n \delta(E_T - n\hbar\omega) \quad (13)$$

A comparison of the two models is provided in Figure 3 for a series of values of the final energy $E_f$ on an inverted-geometry spectrometer, with the two special cases of TOSCA (black lines), $E_f \simeq 3$ meV and VESUVIO (gold lines), with $E_f \simeq 5$ eV. On the top panel of the figure, as the final energy increases, both $E_T$ and $Q$ increase, and $S_{\mathrm{IA}}$ shows a peak, proportional to $J(y)$, centred about $E_R$ and broadened by $\langle E_k \rangle$. The black line


https://dx.doi.org/10.1021/acs.jctc.0c00790
J. Chem. Theory Comput. XXXX, XXX, XXX−XXX

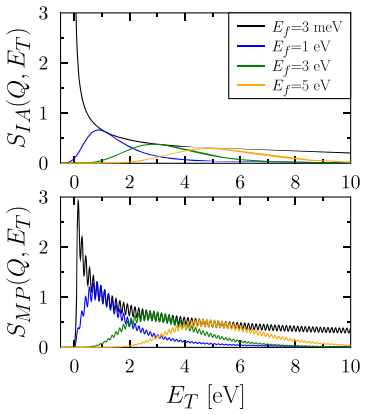


**Figure 3.** Dynamic structure factor in the impulse approximation (top) and in the multiphonon expansion (bottom) as a function of the energy transfer $E_T = E_i - E_f$ for a series of values of the final energy $E_f$.

($E_f$ = 3 meV) is not representative of experimental data, and it is only an extrapolation of eq 11. In fact, the spectra in this case are better represented by eq 13, whose graphical representation is reported on the bottom panel of Figure 3. By comparison of the results from the two equations, one can notice how the modulation of the overtones in the multiphonon expansion of $S_{MP}$ follows the same trend as $S_{IA}$, for all the values of $E_f$. While the single overtones are still visible in the analytic calculation of Figure 3 (bottom), in the experimental spectra, owing to the instrument resolution, the overtones soon combine to form a continuous and flat signal on an INS spectrometer, as one can observe on the right side of Figure 1, or a Gaussian-like peak on a DINS spectrometer.

The ideal equations valid in the IA are generally corrected for final state effects[48] that take into consideration the fact that neither $E_T$ nor $Q$ is infinite in practice. Here, the additive corrections to the NCP[10,15] method are adopted:

$$S_{IA,FSE}(Q, E_T) = S_{IA}\left[1 + \frac{b_3}{Q}H_3(x) + \frac{b_4}{Q^2}H_4(x) + \frac{b_6}{Q^2}H_6(x)\right] \quad (14)$$

where the parameters $b_n$ are functions of $\sigma_p$ in the harmonic approximation,[10] and $H_n(x)$ are the Hermite polynomials, with $x = y/\sqrt{2}\sigma_p$.

Finally, one can express the self-scattering law as

$$\Sigma_{IA,FSE}(Q, E_T) = \frac{\sigma_b}{4\pi}\sqrt{\frac{E_f}{E_i}}S_{IA,FSE}(Q, E_T) \quad (15)$$

Following the discussion in ref 10, one can normalize the INS spectra by imposing the requirement that the experimental intensity in the high energy-transfer region has the same intensity as in eq 11

$$\int_{E_{min}}^{E_{max}} \Sigma_s(Q, E_T)dE_T = \int_{E_{min}}^{E_{max}} \Sigma_{IA,FSE}(Q, E_T)dE_T \quad (16)$$

Considering that this equation only depends on the value of $\sigma_p$ or equivalently of $\langle E_k \rangle$, one can convert the intensity of the INS spectra to a physical scale using the results of a DINS experiment.

### 3.3. Algorithm Implementation.

The aforementioned procedures have been put together in a unique algorithm specifically developed in Python to allow its implementation in MANTID.[49] This choice has been made to allow the neutron scattering community to take advantage of it, since the script presents an user-friendly graphical user interface.

The algorithm, as depicted in Figure 4 via a use case diagram, can be divided into four blocks:

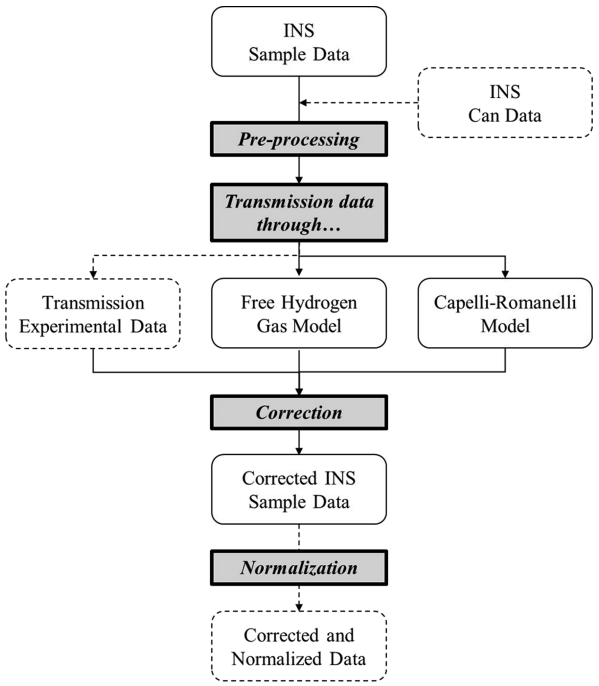


**Figure 4.** Use case diagram of the algorithm, depicting the workflow, the data process, and the four main steps, which are highlighted with a gray background. Optional procedures are shown with dashed lines.

1. INS data import and preprocessing;
2. Transmission data import or transmission modeling;
3. Self-shielding correction;
4. Normalization using $y$-scale formalism.

In INS data import and preprocessing, the INS experimental data are loaded into the script. Depending on the experimental conditions, the user can also load the data (if available) of the INS measurement of the empty sample. If these are provided, in the correction phase, the container signal is subtracted from the experimental data related to the sample enclosed in the container, in order to remove additional contributions provided by the container itself. The container, even if typically made of aluminium that guarantees nearly complete transmission (about 99%), adds an additional attenuation effect on the measurement.

Before being processed, both the sample and the (optional) container data undergo unit conversion because the analyses in the algorithm are provided with energy transfer in meV. The data are then converted to incident energy, $E_i = E_T + E_f$.

In transmission data import or transmission modeling, for the correction procedure, transmission data must be fed into the script. This can be carried out in two different ways (see Figure 4): (a) if transmission data are available, they can be used as a data input to the script and (b) if transmission data are not available, the script allows the user to select either the


https://dx.doi.org/10.1021/acs.jctc.0c00790
J. Chem. Theory Comput. XXXX, XXX, XXX−XXX

FHG model or the Capelli−Romanelli model. The user needs to provide the sample-specific areal density using eq 4. Using any of these two models, the algorithm produces a workspace with the tabulated transmission spectrum.

In self-shielding correction, once the transmission spectrum is available, the algorithm corrects the INS data of the sample according to eqs 1 and 2. The measured signals are then corrected for sample self-shielding and for both sample and container attenuation.

In normalization using $y$-scale formalism, finally, the spectra can be normalized using the $y$-scaling formalism. The user can provide either an experimental value obtained in a DINS experiment or a theoretical value predicted, for example, in a DFT-based simulation and using eq 7. The script requires some additional parameters such as the nuclear mean kinetic energy of hydrogen, the number of hydrogen atoms per unit cell of the sample, and the energy range for the normalization procedure.

After these corrections, INS data coming from different experimental conditions both from the sample and the instrumentation standpoints can be compared for further analysis.

## 4. RESULTS AND DISCUSSION

Results of the DINS data from $ZrH_2$ provide the parameters needed for the normalization of the INS spectra. Figure 5

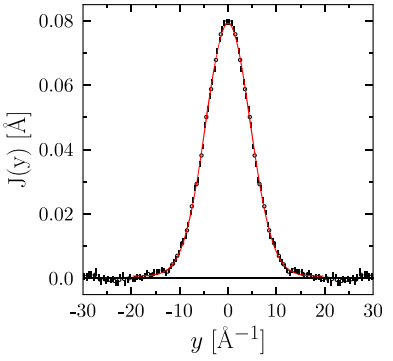


**Figure 5.** Neutron Compton profile of hydrogen in $ZrH_2$ (sample 1, black error bars) at 300 K as measured on VESUVIO, together with its best fit (red solid line).

shows the NCP of hydrogen in sample 1 after the standard data reduction of the DINS data using MANTID,[50] after corrections for environmental-[51,52] and sample-dependent backgrounds,[19,53,54] and convolution with the instrument resolution.[55−57] The analysis provides a value of the total mean kinetic energy of $\langle E_k \rangle = 113 \pm 2$ meV, corresponding to a standard deviation $\sigma_p = 4.22 \pm 0.02$ Å$^{-1}$. The value is in excellent agreement with values previously reported in the literature.[22,58] Concurrent measurements of neutron transmission on VESUVIO (see also Figure 2) are reported for the 1 mm-thick sample in Figure 6 to be compared with the two models. One should first notice how, for neutron energies approaching the epithermal limit ($E_i \rightarrow 1$ eV), the model transmission functions overlap to the experimental one. Theoretically, at epithermal energies, the cross section is no longer affected by phonons or internal vibrations. On a practical side, the model transmissions overlap to the experimental one only if the real sample density is known. As a first guess, the experimenter can define the density from

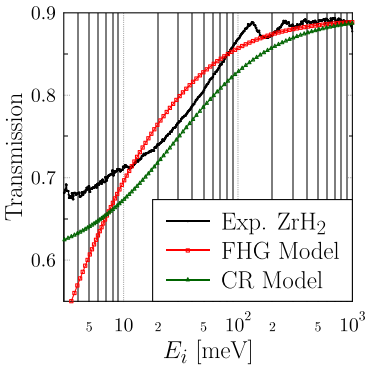


**Figure 6.** Comparison of the three cross section models of the experimental TOSCA and VESUVIO data of $ZrH_2$ of 1 mm in thickness.

the loaded mass of sample in a given volume of the container. However, especially for powder samples, one can expect the sample to rearrange within the container, possibly moving toward the bottom. This was the case in the present experiment where, as opposed to usual experiments, we could monitor the sample distribution within the container using neutron radiography (not shown here). From the radiographs, in the case of the 1 mm-thick sample, we could conclude that the container height was filled only to about 78%, and we corrected the sample density accordingly.

For cold and thermal neutrons, Figure 6 shows drastic differences in the models compared to the experimental spectrum. The model by Capelli and Romanelli (CR) provides a cross section that is always larger than that of $ZrH_2$. This is because organic molecules have more vibrational modes than the 1-phonon density of states of $ZrH_2$. Therefore, the contributions from the multiphonon expansion overlap, and individual contributions are no longer recognized. Moreover, in the limit $E_i \rightarrow 0$, both the CR and experimental functions tend to constant values, driven by the bound scattering cross section of hydrogen. On the other hand, the FHG model suffers from a divergent cross section for vanishing neutron energies, as expected of free atoms not bound to a lattice or molecule.

Figure 7 shows the experimental spectra from sample 1 and sample 2 after the corrections and normalization. The two spectra satisfactorily overlap, showing that the self-shielding corrections were successful. One should notice that the

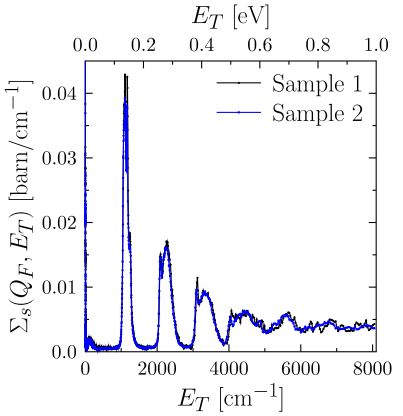


**Figure 7.** Corrected and normalized INS spectra of $ZrH_2$ from sample 1 (black line) and sample 2 (blue line).


https://dx.doi.org/10.1021/acs.jctc.0c00790
J. Chem. Theory Comput. XXXX, XXX, XXX−XXX

intensity of the peak of the first phonon for sample 1 would have been underestimated by ca. 10% if no such corrections would have been performed. A closer inspection shows that, for the thinner sample (sample 1), the peak features are sharper than for the thicker sample (sample 2). This can be related to the presence of multiple scattering in the sample with the higher scattering power. The double scattering can be approximated, as a first approximation, to the convolution of the single-scattering spectrum and the elastic line. Therefore, the result is a replica of the single-scattering spectrum, well represented by sample 1, yet with less-defined features. In this scenario, the presence of multiple scattering does not invalidate the normalization procedure and justifies *a posteriori* the decision to neglect multiple-scattering contributions in eq 1.

**4.1. Application to L-Lysine.** Lysine is an essential amino acid that mammals must acquire from food. The interactions of L-lysine in biological systems are largely dependent on the formation of hydrogen bonds involving the aliphatic side chain and especially the $NH_2$ group.[59,60] Such intermolecular interactions are particularly evident at low values of $E_T$, thus making a proper correction procedure of INS data a fundamental step when comparing to computer simulations.

As an additional test of the correction and normalization procedure, we performed measurements on one L-lysine sample loaded in the same type of TOSCA container with a nominal hydrogen areal density $n_H$ = 0.0081 barn$^{-1}$. The INS spectrum from this sample, corrected and normalized using the INSCorNorm algorithm, is reported in the bottom panel of Figure 8. In particular, this spectrum corresponds to the

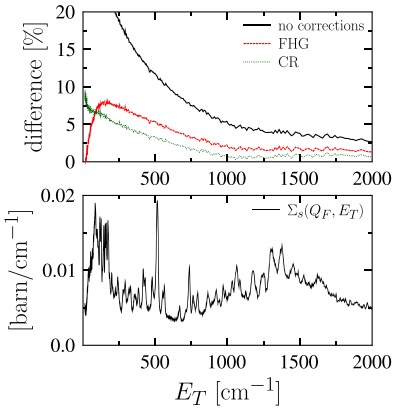


**Figure 8.** Forward-scattering INS spectrum of L-lysine (bottom panel), corrected using the experimental transmission signal and normalized to the absolute scale of barn/cm$^{-1}$ using the INSCorNorm algorithm. The relative differences between this spectrum and the one normalized without corrections (black line) or corrected using the nominal value of $n_H$ and the FHG (red line) or the CR model (green line) are reported in the top panel.

forward-scattering signal and was obtained using the experimental neutron transmission data collected on VESUVIO. For the normalization, we used the experimental value of $\langle E_k \rangle$ = 149.2 ± 0.5 meV, obtained by DINS measurements of the same sample on VESUVIO. In the top panel of Figure 8, we report the relative difference between the abovementioned spectrum and the one normalized either without performing self-attenuation corrections (black line) or using the nominal density and the FHG (red dashed line) or CR model (green dotted line). In this figure, a positive difference corresponds to an underestimate of the vibrational intensity with respect to the correction procedure based on the experimental transmission spectra. One can notice how, for $E_T \simeq 500$ cm$^{-1}$, the intensity of the vibrational modes is underestimated by about 10% and increases more as one approaches the elastic line, in the region where hydrogen-bonding fingerprints are expected. When the data are corrected, either with the FHG or with the CR models, the relative difference with the properly reduced data is lower. In most of the energy range reported in the figure, the CR model provides better results than the FHG model, as one should expect from the organic nature of the sample. In this case, the difference can be mainly related to the lower value of the nominal hydrogen areal density with respect to the effective one directly probed in the experimental transmission data. It is interesting to notice in Figure 8 the crossing point of the CR and FHG models at around 100 cm$^{-1}$. The existence of this crossing point, due to the different dependence of $\sigma(E)$ in the two models upon the incident neutron energy, had been anticipated in Figure 6.

It is important to note that atom-projected vibrational densities of states are routinely used to evaluate anisotropic displacement parameters (ADPs), for example, in molecular crystals.[61,62] Owing to the $1/E_T$ dependence of the ADPs, the underestimate of the intensities of the modes in the lowest energy range of the INS spectra is tantamount to a substantial underestimate of the ADPs. Therefore, the INS spectra corrected using the INSCorNorm algorithm provide robust support to benchmarking phonon-based calculations of ADPs and the related analysis of X-ray and neutron diffraction data.

## 5. CONCLUSIONS

In this work, the algorithm INSCorNorm has been described and applied. It is a python-based procedure for the correction and physical normalization of the INS spectra collected on the TOSCA spectrometer. The algorithm can be used self-consistently with the experimental transmission spectra, for the corrections, and values of the proton mean kinetic energy, for the normalization, measured on the VESUVIO spectrometer. Alternatively, one can make use of two model functions for the sample cross section of which one is suitable for organic samples. A practical example for $ZrH_2$ at 300 K has been discussed. Moreover, we have applied the algorithm to INS data from L-lysine, an organic system of broad interest in medicine and biology, and we have discussed how properly corrected spectra can provide a useful benchmark for theoretical investigations probing intermolecular interactions and predicting anisotropic displacement parameters.

While the results have been presented in the case of the TOSCA spectrometer, the algorithm can be applied to results from any inverted-geometry instrument.[10] Importantly, next-generation INS spectrometers[63] would greatly benefit from concurrent energy-selective neutron transmission measurements over the same energy range probed in the vibrational spectra. Such capability would allow a self-consistent correction of the data using the experimental attenuation of the sample, thus taking into account subtle dependencies upon temperature and other sample-environment stimuli.

## AUTHOR INFORMATION

**Corresponding Author**

**Giovanni Romanelli** − *ISIS Facility, Rutherford Appleton Laboratory, Didcot, Oxfordshire OX11 0QX, U.K.;*
orcid.org/0000-0001-5963-4647;
Email: giovanni.romanelli@stfc.ac.uk



https://dx.doi.org/10.1021/acs.jctc.0c00790
J. Chem. Theory Comput. XXXX, XXX, XXX−XXX

## Authors

**Claudia Scatigno** − *Dipartimento di Scienze Fisiche e Tecnologie della Materia, CNR, 00185 Roma, Italy; Museo Storico della Fisica e Centro Studi e Ricerche Enrico Fermi, 00184 Rome, Italy*

**Enrico Preziosi** − *Dipartimento di Fisica e NAST Centre, Università degli Studi di Roma "Tor Vergata", 00133 Rome, Italy*

**Matteo Zanetti** − *Dipartimento di Scienze Fisiche e Tecnologie della Materia, CNR, 00185 Roma, Italy; Advanced Nuclear Systems, SCK-CEN, 2400 Mol, Belgium*

**Stewart F. Parker** − *ISIS Facility, Rutherford Appleton Laboratory, Didcot, Oxfordshire OX11 0QX, U.K.;* orcid.org/0000-0002-3228-2570

**Svemir Rudić** − *ISIS Facility, Rutherford Appleton Laboratory, Didcot, Oxfordshire OX11 0QX, U.K.*

**Carla Andreani** − *Dipartimento di Fisica e NAST Centre, Università degli Studi di Roma "Tor Vergata", 00133 Rome, Italy*

**Roberto Senesi** − *Dipartimento di Fisica e NAST Centre, Università degli Studi di Roma "Tor Vergata", 00133 Rome, Italy; CNR-IPCF, 98158 Messina, Italy*

Complete contact information is available at: https://pubs.acs.org/10.1021/acs.jctc.0c00790

## Notes

The authors declare no competing financial interest.

## ■ ACKNOWLEDGMENTS

The authors gratefully acknowledge the financial support of Regione Lazio (IR approved by Giunta Regionale n. G10795, 7 August 2019 published by BURL n. 69 27 August 2019), ISIS@MACH (I), and ISIS Neutron and Muon Source (UK) of Science and Technology Facilities Council (STFC); the financial support of Consiglio Nazionale delle Ricerche within CNR-STFC Agreement 2014-2020 (N 3420), concerning collaboration in scientific research at the ISIS Neutron and Muon Source (UK) of Science and Technology Facilities Council (STFC), and the ESS-ERIC for Instrument VESPA Phase 1 are gratefully acknowledged.

## ■ REFERENCES

(1) Mitchell, P. C. H.; Parker, S. F.; Ramirez-Cuesta, A. J.; Tomkinson, J. *Vibrational spectroscopy with neutrons: with applications in chemistry, biology, materials science and catalysis*; World Scientific: Singapore, 2005, DOI: 10.1142/5628

(2) Parker, S. F.; Carlile, C. J.; Pike, T.; Tomkinson, J.; Newport, R. J.; Andreani, C.; Ricci, F. P.; Sacchetti, F.; Zoppi, M. TOSCA: a world class inelastic neutron spectrometer. *Phys. B* **1997**, *241-243*, 154−156.

(3) *ISIS Neutron and Muon Source, Science and Technology Facilities Council*, ISIS INS Database. 2020; https://www.isis.stfc.ac.uk/Pages/INS-database.aspx, Last access on July 2020

(4) Rudic, S.; Ramirez-Cuesta, A. J.; Parker, S. F.; Fernandez-Alonso, F.; Pinna, R. S.; Gorini, G.; Salzmann, C. G.; McLain, S. E.; Skipper, N. T. TOSCA international beamline review. *RAL Technical Reports RAL-TR-2013-015*; STFC: 2013

(5) Pinna, R. S.; Rudić, S.; Parker, S. F.; Armstrong, J.; Zanetti, M.; Škoro, G.; Waller, S. P.; Zacek, D.; Smith, C. A.; Capstick, M. J.; McPhail, D. J.; Pooley, D. E.; Howels, G. D.; Gorini, G.; Fernandez-Alonso, F. The neutron guide upgrade of the TOSCA spectrometer. *Nucl. Instrum. Methods Phys. Res., Sect. A* **2018**, *896*, 68−74.

(6) Pinna, R. S.; Rudić, S.; Parker, S. F.; Gorini, G.; Fernandez-Alonso, F. Monte carlo simulations of the TOSCA spectrometer: Assessment of current performance and future upgrades. *EPJ Web Conf.* **2015**, *83*, No. 03013.

(7) Parker, S. F.; Fernandez-Alonso, F.; Ramirez-Cuesta, A. J.; Tomkinson, J.; Rudic, S.; Pinna, R. S.; Gorini, G.; Castañon, J. F. Recent and future developments on TOSCA at ISIS. *J. Phys.: Conf. Ser.* **2014**, *554*, No. 012003.

(8) Tomkinson, J.; Penfold, J.; Robertson, S. T. *The optic modes in $ZrH_2$*. RAL Technical Report RAL-89-074: 1989

(9) Couch, J. G.; Harling, O. K.; Clune, L. C. Structure in the neutron scattering spectra of zirconium hydride. *Phys. Rev. B* **1971**, *4*, 2675.

(10) Colognesi, D. The high energy-transfer region in neutron scattering vibrational spectra: What does it mean and what could it be useful for? *J. Neutron Res.* **2017**, *19*, 147−167.

(11) West, G. B. Electron scattering from atoms, nuclei and nucleons. *Phys. Rep.* **1975**, *18*, 263−323.

(12) Sears, V. F. Scaling and final-state interactions in deep-inelastic neutron scattering. *Phys. Rev. B* **1984**, *30*, 44.

(13) Gunn, J. M. F.; Andreani, C.; Mayers, J. A new approach to impulsive neutron scattering. *J. Phys. C: Solid State Phys.* **1986**, *19*, L835.

(14) Andreani, C.; Colognesi, D.; Mayers, J.; Reiter, G. F.; Senesi, R. Measurement of momentum distribution of light atoms and molecules in condensed matter systems using inelastic neutron scattering. *Adv. Phys.* **2005**, *54*, 377−469.

(15) Andreani, C.; Krzystyniak, M.; Romanelli, G.; Senesi, R.; Fernandez-Alonso, F. Electron-volt neutron spectroscopy: beyond fundamental systems. *Adv. Phys.* **2017**, *66*, 1−73.

(16) Andreani, C.; Senesi, R.; Krzystyniak, M.; Romanelli, G.; Fernandez-Alonso, F. Atomic quantum dynamics in materials research. *Exp. Methods Phys. Sci.* **2017**, *49*, 403−457.

(17) Senesi, R.; Andreani, C.; Bowden, Z.; Colognesi, D.; Degiorgi, E.; Fielding, A. L.; Mayers, J.; Nardone, M.; Norris, J.; Praitano, M.; Rhodes, N. J.; Stirling, W. G.; Tomkinson, J.; Uden, C. VESUVIO: a novel instrument for performing spectroscopic studies in condensed matter with eV neutrons at the ISIS facility. *Phys. B* **2000**, *276-278*, 200−201.

(18) Andreani, C.; Pietropaolo, A.; Senesi, R.; Gorini, G.; Tardocchi, M.; Bracco, A.; Rhodes, N.; Schooneveld, E. Electron-volt spectroscopy at a pulsed neutron source using a resonance detector technique. *Nucl. Instrum. Methods Phys. Res., Sect. A* **2002**, *481*, 509−520.

(19) Gorini, G.; Perelli-Cippo, E.; Tardocchi, M.; Andreani, C.; D'Angelo, A.; Pietropaolo, A.; Senesi, R.; Imberti, S.; Bracco, A.; Previtali, E.; Pessina, G.; Rhodes, N. J.; Schooneveld, E. M. The resonant detector and its application to epithermal neutron spectroscopy. *Nucl. Instrum. Methods Phys. Res., Sect. A* **2004**, *529*, 293−300.

(20) Mayers, J.; Tomkinson, J.; Abdul-Redah, T.; Stirling, W. G.; Andreani, C.; Senesi, R.; Nardone, M.; Colognesi, D.; Degiorgi, E. VESUVIO-the double difference inverse geometry spectrometer at ISIS. *Phys. B* **2004**, *350*, E659−E662.

(21) Pietropaolo, A.; Andreani, C.; Filabozzi, A.; Senesi, R.; Gorini, G.; Perelli-Cippo, E.; Tardocchi, M.; Rhodes, N. J.; Schooneveld, E. M. DINS measurements on VESUVIO in the Resonance Detector configuration: proton mean kinetic energy in water. *J. Instrum.* **2006**, *1*, P04001.

(22) Mayers, J.; Reiter, G. The VESUVIO electron volt neutron spectrometer. *Meas. Sci. Technol.* **2012**, *23*, No. 045902.

(23) Rodríguez Palomino, L. A.; Dawidowski, J.; Márquez Damián, J. I.; Cuello, G. J.; Romanelli, G.; Krzystyniak, M. Neutron total cross-section of hydrogenous and deuterated 1-and 2-propanol and n-butanol measured using the VESUVIO spectrometer. *Nucl. Instrum. Methods Phys. Res., Sect. A* **2017**, *870*, 84−89.

(24) Romanelli, G.; Rudić, S.; Zanetti, M.; Andreani, C.; Fernandez-Alonso, F.; Gorini, G.; Krzystyniak, M.; Škoro, G. Measurement of the para-hydrogen concentration in the ISIS moderators using neutron transmission and thermal conductivity. *Nucl. Instrum. Methods Phys. Res., Sect. A* **2018**, *888*, 88−95.

(25) Capelli, S. C.; Romanelli, G. An effective hydrogen scattering cross section for time-of-flight neutron experiments with simple organic molecules. *J. Appl. Crystallogr.* **2019**, *52*, 1233−1237.
(26) Rodríguez Palomino, L. A.; Dawidowski, J.; Helman, C.; Márquez Damián, J. I.; Romanelli, G.; Krzystyniak, M.; Rudić, S.; Cuello, G. J. Determination of the scattering cross section of calcium using the VESUVIO spectrometer. *Nucl. Instrum. Methods Phys. Res., Sect. A* **2019**, *927*, 443−450.
(27) Romanelli, G.; Krzystyniak, M.; Senesi, R.; Raspino, D.; Boxall, J.; Pooley, D.; Moorby, S.; Schooneveld, E.; Rhodes, N. J.; Andreani, C.; Fernandez-Alonso, F. Characterisation of the incident beam and current diffraction capabilities on the VESUVIO spectrometer. *Meas. Sci. Technol.* **2017**, *28*, No. 095501.
(28) Robledo, J. I.; Dawidowski, J.; Márquez Damián, J. I.; Škoro, G.; Bovo, C.; Romanelli, G. Measurement of neutron total cross sections at the VESUVIO spectrometer. *Nucl. Instrum. Methods Phys. Res., Sect. A* **2020**, 164096.
(29) Krzystyniak, M.; Romanelli, G.; Fabian, M.; Gutmann, M.; Festa, G.; Arcidiacono, L.; Gigg, M.; Drubicki, K.; Andreani, C.; Senesi, R.; Fernandez-Alonso, F. VESUVIO+: The Current Testbed for a Next-generation Epithermal Neutron Spectrometer. *J. Phys.: Conf. Ser.* **2018**, *1021*, No. 012026.
(30) Evans, A. C.; Timms, D. N.; Mayers, J.; Bennington, S. M. Neutron-scattering study of the impulse approximation in $ZrH_2$. *Phys. Rev. B* **1996**, *53*, 3023.
(31) Scatigno, C.; Zanetti, M.; Rudic, S.; Gorini, G.; Fernandez-Alonso, F.; Andreani, C.; Senesi, R. Quantitative Benchmarks of state-of-art Neutron Chemical Spectrometers - Part 1: TOSCA. *ISIS Neutron and Muon Source Data Journal*; STFC ISIS Neutron and Muon Source: 2018.
(32) Nelson, D.; Cox, M. *Lehninger Principles of Biochemistry*; (4th Ed.); W.H. Freeman and Company: New York, 2005
(33) Wang, Z. A.; Cole, P. A. The Chemical Biology of Reversible Lysine Post-translational Modifications. *Cell Chem. Biol.* **2020**, 953.
(34) Feuz, L.; Strunz, P.; Geue, T.; Textor, M.; Borisov, O. Conformation of poly (L-lysine)-graft-poly (ethylene glycol) molecular brushes in aqueous solution studied by small-angle neutron scattering. *Eur. Phys. J. E* **2007**, *23*, 237−245.
(35) Zanetti, M.; Gorini, G.; Romanelli, G.; Scatigno, C.; Andreani, C.; Senesi, R.; Fernandez-Alonso, F. Quantitative Benchmarks of state-of-art Neutron Chemical Spectrometers - Part 2: VESUVIO. *ISIS Neutron and Muon Source Data Journal*; STFC ISIS Neutron and Muon Source: 2018.
(36) Pinna, R. S.; Rudić, S.; Capstick, M. J.; McPhail, D. J.; Pooley, D. E.; Howells, G. D.; Gorini, G.; Fernandez-Alonso, F. Detailed characterisation of the incident neutron beam on the TOSCA spectrometer. *Nucl. Instrum. Methods Phys. Res., Sect. A* **2017**, *870*, 79−83.
(37) Pietropaolo, A.; Andreani, C.; Rebai, M.; Giacomelli, L.; Gorini, G.; Perelli Cippo, E.; Tardocchi, M.; Fazzi, A.; Verona Rinati, G.; Verona, C.; Marinelli, M.; Milani, E.; Frost, C. D.; Schooneveld, E. M. Fission diamond detectors for fast-neutron ToF spectroscopy. *Europhys. Lett.* **2011**, *94*, 62001.
(38) Tardocchi, M.; Pietropaolo, A.; Andreani, C.; Bracco, A.; D'Angelo, A.; Gorini, G.; Imberti, S.; Senesi, R.; Rhodes, N. J.; Schooneveld, E. M. Cadmium-Zinc-Telluride photon detector for epithermal neutron spectroscopy-pulse height response characterisation. *Nucl. Instrum. Methods Phys. Res., Sect. A* **2004**, *526*, 477−492.
(39) Andreani, C.; Pietropaolo, A.; Senesi, R.; Gorini, G.; Perelli-Cippo, E.; Tardocchi, M.; Rhodes, N.; Schooneveld, E. M. A resonant detector for high-energy inelastic neutron scattering experiments. *Appl. Phys. Lett.* **2004**, *85*, 5454.
(40) Andreani, C.; Romanelli, G.; Senesi, R. Direct Measurements of Quantum Kinetic Energy Tensor in Stable and Metastable Water near the Triple Point: An Experimental Benchmark. *J. Phys. Chem. Lett.* **2016**, *7*, 2216−2220.
(41) Andreani, C.; Senesi, R.; Krzystyniak, M.; Romanelli, G.; Fernandez-Alonso, F. Experimental studies of nuclear quantum effects in condensed matter: The case of water. *Riv. Nuovo Cimento* **2018**, *41*, 291−340.
(42) Romanelli, G.; Senesi, R.; Zhang, X.; Loh, K. P.; Andreani, C. Probing the effects of 2D confinement on hydrogen dynamics in water and ice adsorbed in graphene oxide sponges. *Phys. Chem. Chem. Phys.* **2015**, *17*, 31680−31684.
(43) Romanelli, G.; Liscio, A.; Senesi, R.; Zamboni, R.; Treossi, E.; Liscio, F.; Giambastiani, G.; Palermo, V.; Fernandez-Alonso, F.; Andreani, C. Soft confinement of water in graphene-oxide membranes. *Carbon* **2016**, *108*, 199−203.
(44) De Michele, V.; Romanelli, G.; Cupane, A. Dynamics of supercooled confined water measured by deep inelastic neutron scattering. *Front. Phys.* **2018**, *13*, 138205.
(45) Agrawal, A. K. Multiple scattering of neutrons in gaseous and liquid methane. *Phys. Rev. A* **1971**, *4*, 1560.
(46) Fernandez-Alonso, F.; Price, D. L. *Neutron Scattering*; Academic Press: 2013
(47) Watson, G. I. Neutron compton scattering. *J. Phys.: Condens. Matter* **1996**, *8*, 5955.
(48) Pace, E.; Salmè, G.; West, G. Final state interaction in quasi-elastic electron scattering by nuclei and y scaling. *Phys. Lett. B* **1991**, *273*, 205−210.
(49) Arnold, O.; Bilheux, J. C.; Borreguero, J. M.; Buts, A.; Campbell, S. I.; Chapon, L.; Doucet, M.; Draper, N.; Ferraz Leal, R.; Gigg, M. A.; Lynchc, V. E.; Markvardsena, A.; Mikkelsonec, D. J.; Mikkelsonec, R. L.; Millerf, R.; Palmena, K.; Parkera, P.; Passosa, G.; Zikovskyc, J. J. Mantid−Data analysis and visualization package for neutron scattering and $\mu$ SR experiments. *Nucl. Instrum. Methods Phys. Res., Sect. A* **2014**, *764*, 156−166.
(50) Romanelli, G.; Hewer, B.; Krzystyniak, M.; Gigg, M.; Tolchenov, R.; Mukhopadhyay, S.; Fernandez-Alonso, F. Data analysis of neutron Compton scattering experiments using MANTID. *J. Phys.: Conf. Ser.* **2018**, *1055*, No. 012016.
(51) Pietropaolo, A.; Andreani, C.; D'Angelo, A.; Senesi, R.; Gorini, G.; Imberti, S.; Tardocchi, M.; Rhodes, N.; Schooneveld, E. S. $\gamma$ detectors for Deep Inelastic Neutron Scattering in the 1-100 eV energy region. *Appl. Phys. A* **2002**, *74*, s189−s190.
(52) Pietropaolo, A.; Perelli Cippo, E.; Gorini, G.; Tardocchi, M.; Schooneveld, E. M.; Andreani, C.; Senesi, R. $\gamma$-Ray background sources in the VESUVIO spectrometer at ISIS spallation neutron source. *Nucl. Instrum. Methods Phys. Res., Sect. A* **2009**, *608*, 121−124.
(53) Schooneveld, E. M.; Mayers, J.; Rhodes, N. J.; Pietropaolo, A.; Andreani, C.; Senesi, R.; Gorini, G.; Perelli-Cippo, E.; Tardocchi, M. Foil cycling technique for the VESUVIO spectrometer operating in the resonance detector configuration. *Rev. Sci. Instrum.* **2006**, *77*, No. 095103.
(54) Mayers, J.; Fielding, A. L.; Senesi, R. *Nucl. Instrum. Methods Phys. Res., Sect. A* **2002**, *481*, 454.
(55) Andreani, C.; Baciocco, G.; Holt, R. S.; Mayers, J. Resolution in deep inelastic neutron scattering using pulsed neutron sources. *Nucl. Instrum. Methods Phys. Res., Sect. A* **1989**, *276*, 297−305.
(56) Imberti, S.; Andreani, C.; Garbuio, V.; Gorini, G.; Pietropaolo, A.; Senesi, R.; Tardocchi, M. Resolution of the VESUVIO spectrometer for High-energy Inelastic Neutron Scattering experiments. *Nucl. Instrum. Methods Phys. Res., Sect. A* **2005**, *552*, 463.
(57) Pietropaolo, A.; Andreani, C.; Filabozzi, A.; Pace, E.; Senesi, R. Resolution function in deep inelastic neutron scattering using the Foil Cycling Technique. *Nucl. Instrum. Methods Phys. Res., Sect. A* **2007**, *570*, 498−510.
(58) Prisk, T. R.; Kolesnikov, A. I.; Granroth, G. E.; Lin, J.-L.; Heuser, B. J. Vibrational modes and quantum zero-point energy of hydrogen in ZrH0.0155 and ZrH2. *J. Alloys Compd.* **2020**, *818*, 152832.
(59) Boeckx, B.; Maes, G. Experimental and Theoretical Observation of Different Intramolecular H-bonds in Lysine Conformations. *J. Phys. Chem. B* **2012**, *116*, 12441−12449.
(60) Stearns, J. A.; Seaiby, C.; Boyarkin, O. V.; Rizzo, T. R. Spectroscopy and conformational preferences of gas-phase helices. *Phys. Chem. Chem. Phys.* **2009**, *11*, 125−132.


https://dx.doi.org/10.1021/acs.jctc.0c00790
J. Chem. Theory Comput. XXXX, XXX, XXX−XXX

(61) Madsen, A. Ø.; Civalleri, B.; Ferrabone, M.; Pascale, F.; Erba, A. Anisotropic displacement parameters for molecular crystals from periodic Hartree−Fock and density functional theory calculations. *Acta Crystallogr., Sect. A: Found. Crystallogr.* **2013**, *69*, 309−321.
(62) George, J.; Wang, A.; Deringer, V. L.; Wang, R.; Dronskowski, R.; Englert, U. Anisotropic displacement parameters from dispersion-corrected DFT methods and their experimental validation by temperature-dependent X-ray diffraction. *CrystEngComm* **2015**, *17*, 7414−7422.
(63) Zanetti, M.; Bellissima, S.; del Rosso, L.; Masi, F.; Chowdhury, M.; De Bonis, A.; Di Fresco, L.; Scatigno, C.; Armstrong, J.; Rudić, S.; Parker, S. F.; Hartl, M.; Colognesi, D.; Senesi, R.; Andreani, C.; Gorini, G.; Fernandez-Alonso, F. Neutronic developments on TOSCA and VESPA: Progress to date. *Phys. B* **2019**, *562*, 107−111.


https://dx.doi.org/10.1021/acs.jctc.0c00790
*J. Chem. Theory Comput.* XXXX, XXX, XXX−XXX